Global Biogeochemical Cycles

Supporting Information for

Joint CO2 Mole Fraction and Flux Analysis Confirms Missing Processes in CASA Terrestrial Carbon Uptake over North America

Sha Feng[1], Thomas Lauvaux[1,2], Christopher A. Williams[3], Kenneth J. Davis[1,5], Yu Zhou[3], Ian Baker[4], Zachary R. Barkley[1], Daniel Wesloh[1]

[1]Department of Meteorology and Atmospheric Science, The Pennsylvania State University, University Park, PA, USA

[2]Laboratoire des Sciences du Climat et de l'Environnement, CEA, CNRS, UVSQ/IPSL, Université Paris-Saclay, Orme des Merisiers, 91191 Gif-sur-Yvette cedex, France

[3]Graduate School of Geography, Clark University, Worcester, MA, USA

[4]Cooperative Institute for Research in the Atmosphere, Colorado State University, Fort Collins, CO, US

[5]Earth and Environmental Systems Institute, The Pennsylvania State University, University Park, Pennsylvania, USA

Contents of this file

Text S1. Model performance: Nudged run vs. free run

We chose to nudge WRF-Chem to the ERA5 analysis to constrain model transport and aimed to reduce the transport uncertainty in modeled CO2. Figure S1 shows the wind biases from the nudged and free simulations against the National Oceanic and Atmospheric Administration (NOAA) rawindsonde data (https://ruc. noaa.gov/raobs/). Here we only include the evaluation of Atmospheric boundary layer (ABL) wind for simplicity. The wind field at 950 hPa is used to represent the ABL. Both used the same model physics as transport run #1 shown in Table 2 in the main text. The comparison of the simulated wind speed and direction between these two runs shows that the observation constraint largely reduces the model transport errors.

Text S2. Diel cycle of the tower footprints

The [CO2] towers carry a long memory of the atmospheric signals as opposed to the flux towers. We chose release particles in LPDM at 21 UTC every day to demonstrate the diel cycle of the influence of the [CO2] towers (Figure S2) to represent the daytime condition for simplicity (Figure S3). The signals exponentially decay within the prior 4 hours of the measuring time, quickly dropping from 30 % to 12 % on average. The fraction of the signals remains around 12 % back to the 20th hour of the previous day when the ABL collapses, after which the fraction of the signals drops again below 10 %. Further back in time, the fraction remains below 10 %. After averaging, the influence of a certain hour to the measuring time is almost the same. The daytime hours only contribute about 1% more signal than nighttime hours. We therefore use equal weights in time when we construct the flux bias for each [CO2] tower.

Supporting Figures:

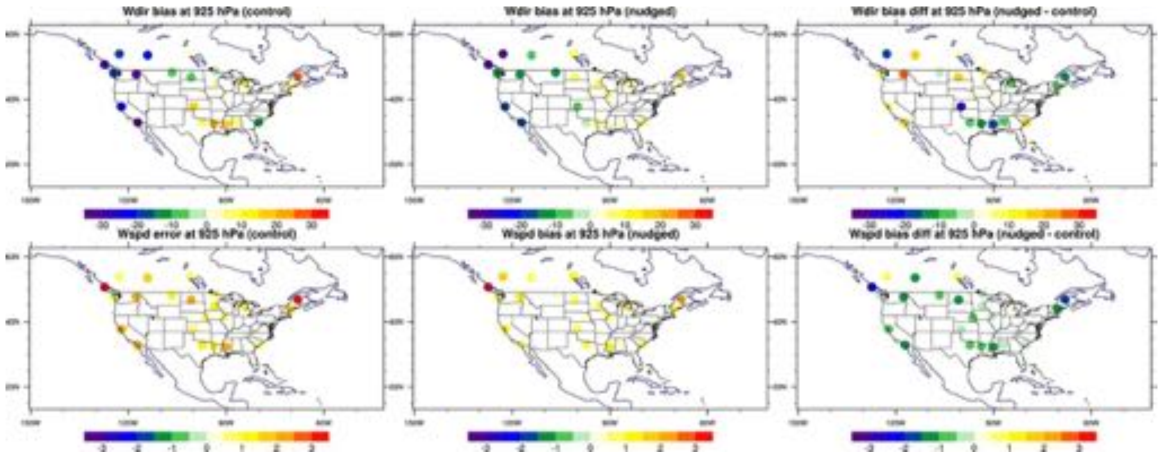

Figure S1. 950 hPa Wind direction (upper; unit in degree) and speed (bottom; unit in m/s) biases in the nudged and free control simulations and their differences (nudged – control)

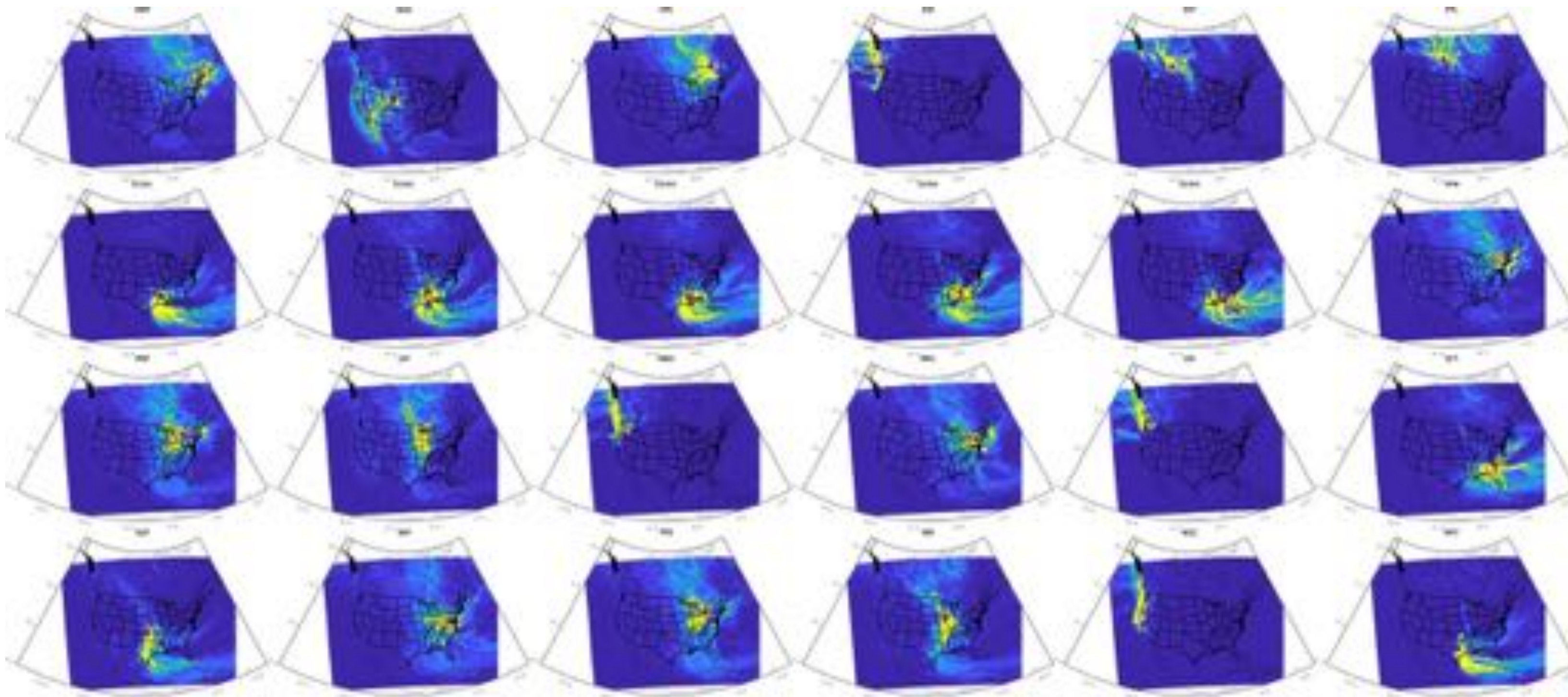

Figure S2. Two-week averaged influence area (footprint) of [CO2] towers. Red dots denote the tower locations.

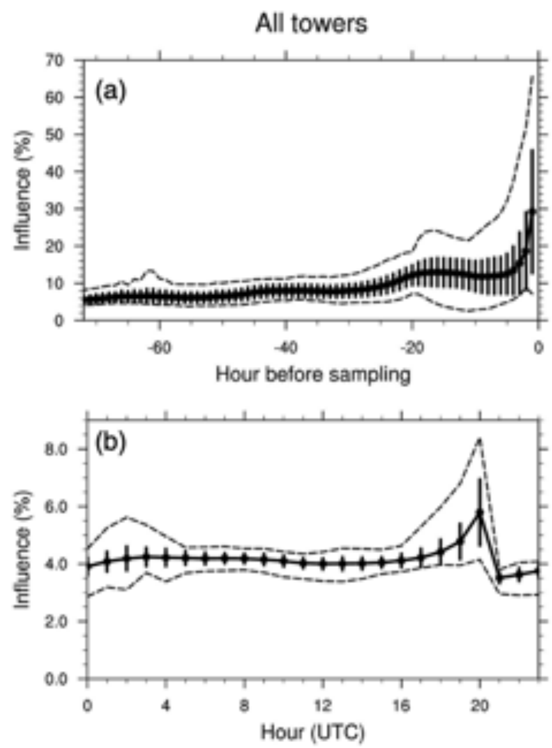

Figure S3. (a) Normalized tower footprint as function of time prior to the particle release at 21 UTC of day. (b) Two-week averaged relative influence for hour of day when the particle release at 21 UTC of day.

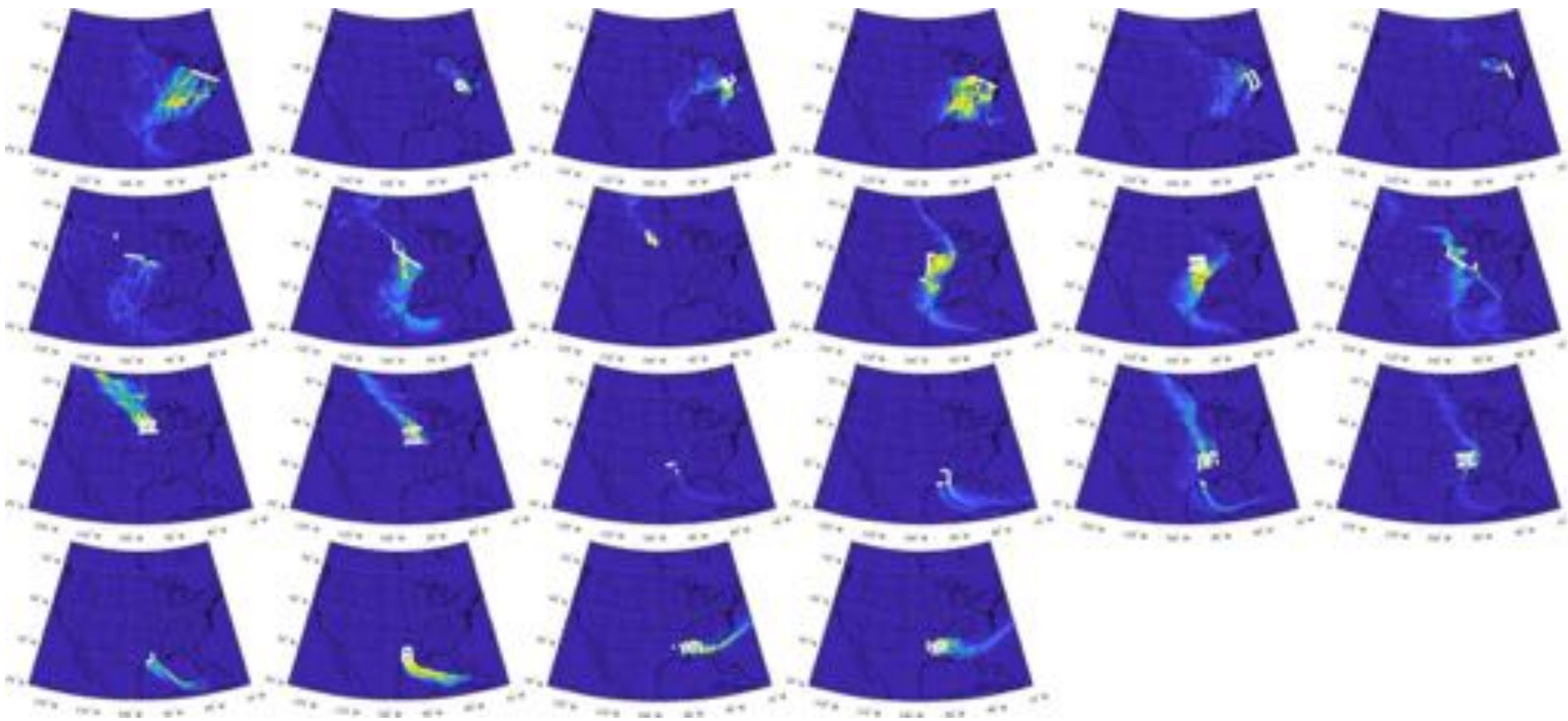

Figure S4. Two-week averaged influence area (footprint) of aircraft ABL legs. White lines denote the aircraft leg locations.

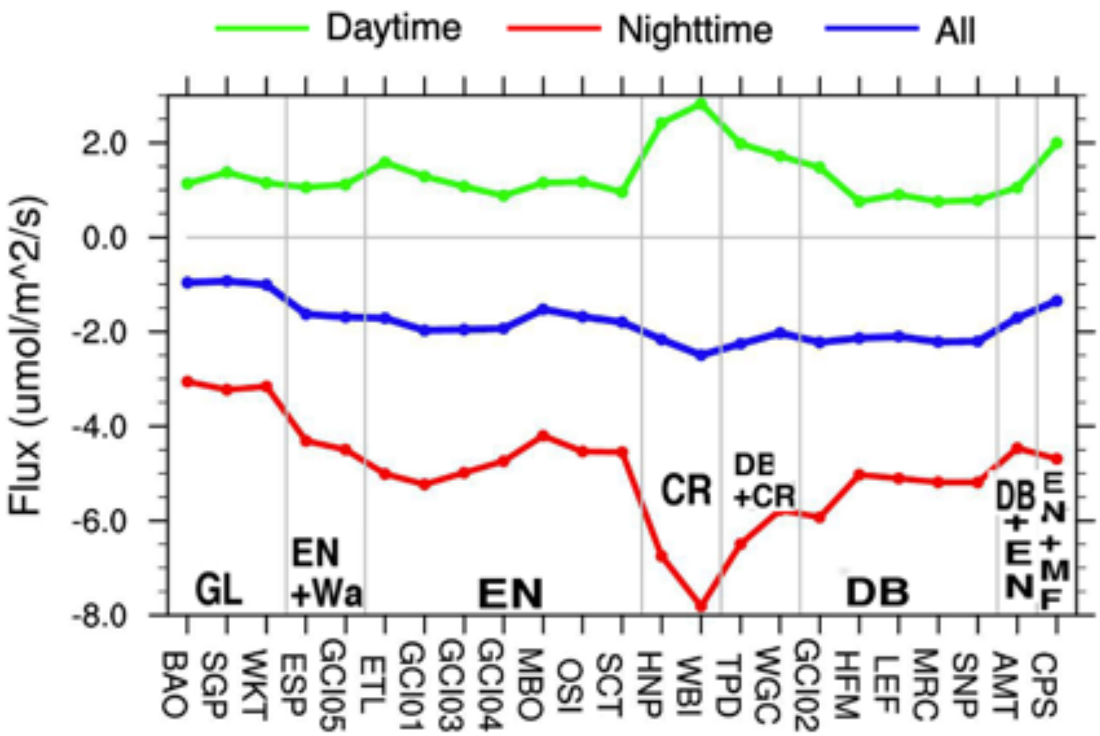

Figure S5. Six-week averaged flux-tower observations paired with every [CO2] tower using Eq. (1) in the main text.

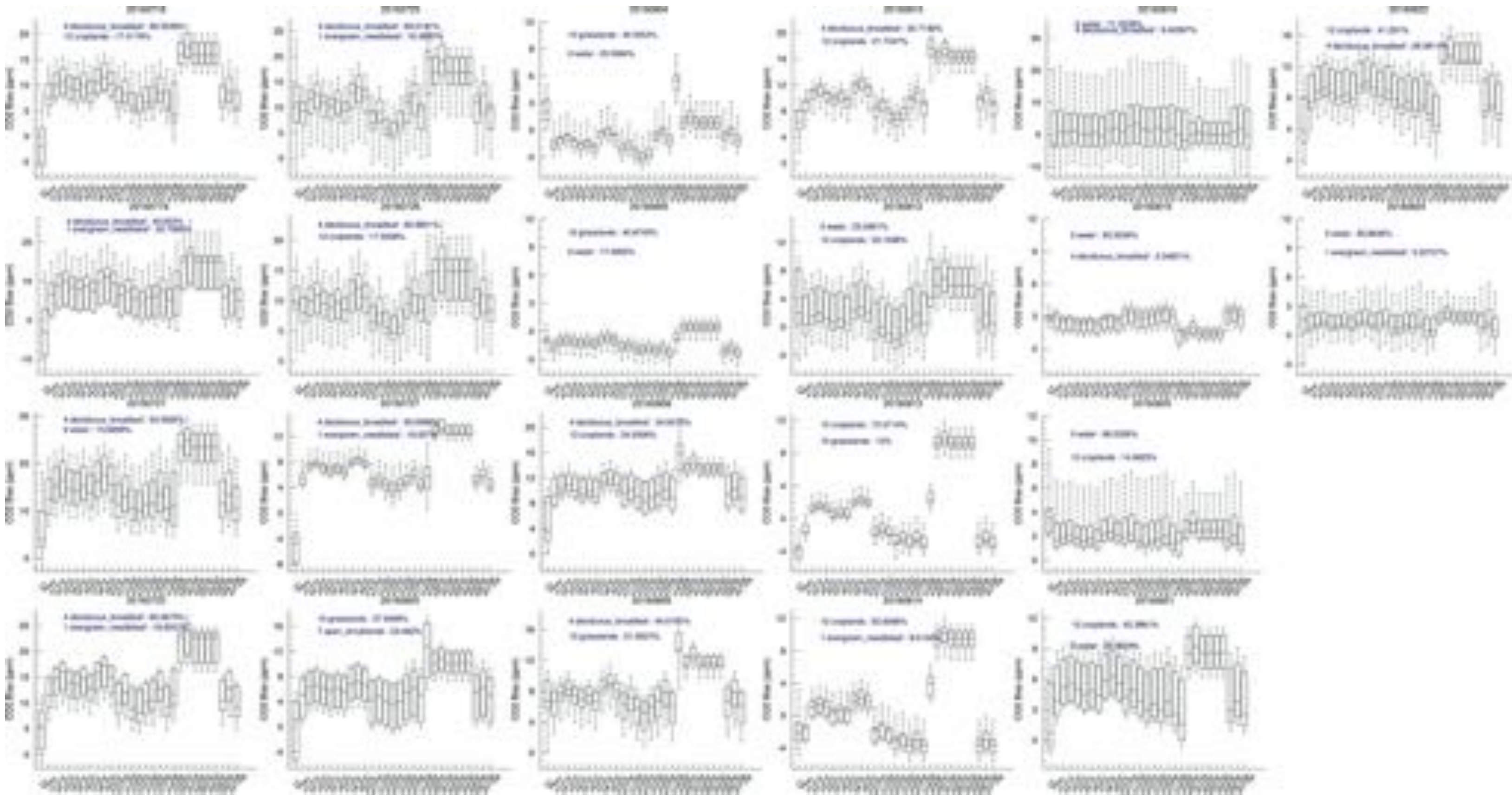

Figure S6. The boxplots of modeled [CO_2] biases associated with individual CASA flux ensemble members and CT2017. The lower and upper ends of each box represent 25% and 75% quartiles of the data points that are modeled [CO_2] biases from all transport and boundary condition ensemble simulations. The two biome types with the greatest influence on the given aircraft samples and the related fraction are marked in each panel.

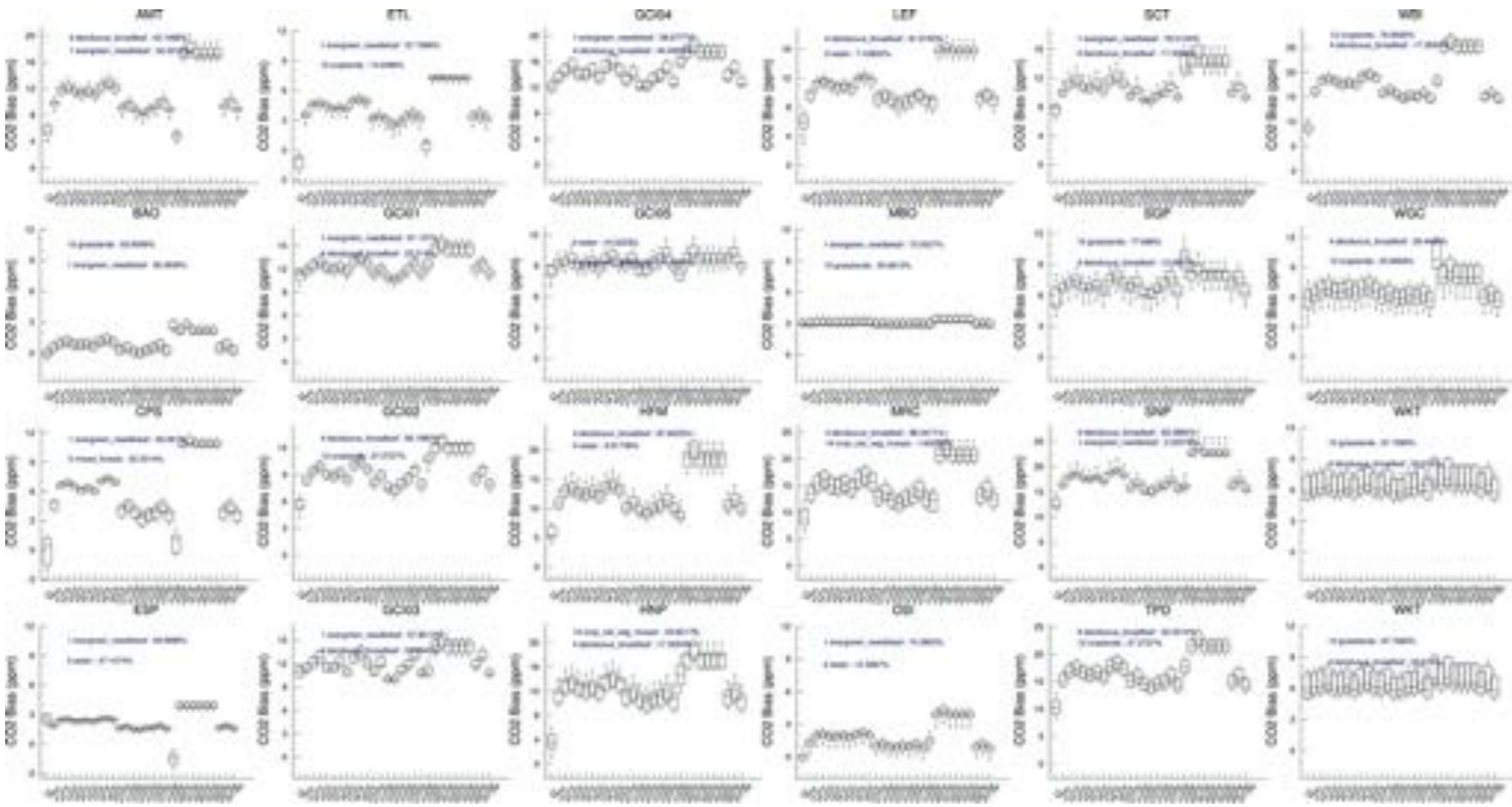

Figure S7. Same as Figure S6 but for the comparison with [CO_2] tower data.

Supporting Tables:

Table S1. ACT-America summer 2016 campaign catalog

Date	Region	Flight patterns
2016-07-18*	MA	Cold front crossing flight
2016-07-19	MA	Cold front crossing flight
2016-07-21*	MA	Fair weather flight day 1
2016-07-22	MA	Fair weather flight day 2
2016-07-25	MA	Cold front crossing flight
2016-07-26	MA	Cold front crossing flight
2016-07-27	MA	Fair weather flight
2016-08-01	MA to MW transit	Transit flight (no samples)
2016-08-03	MW	Cold front crossing flight
2016-08-04*	MW	Cold front crossing flight
2016-08-05	MW	Fair weather flight
2016-08-08	MW	Stationary frontal boundary crossing flight
2016-08-09*	MW	Fair weather flight day 1
2016-08-10	MW	Fair weather flight day 2
2016-08-12	MW	Frontal crossing flight
2016-08-13	MW	Fair weather flight day 1
2016-08-14	MW	Fair weather flight day 2
2016-08-16	MW to South transit	Cold front crossing flight
2016-08-19	South	Gulf of Mexico (GoM) inflow flight
2016-08-20	South	Hybrid: GoM inflow flight pattern and cold front crossing flight
2016-08-21	South	Hybrid: Cold front crossing flight in the west and GoM inflow box in the east sector
2016-08-22*	South	Fair weather flight
2016-08-23	South	GoM inflow flight pattern
2016-08-24	South	Fair-weather box pattern and sampling of GoM inflow

More details about flight catalog can be found at https://actamerica.ornl.gov/campaigns.html#SUMMER_2016

Table S2. Selected AmeriFlux flux towers

Site	Latitude	Longitude	Elevation (m)	Doi
US-A32	36.82	-97.82	335	https://doi.org/10.17190/AMF/1436327
US-A74	36.81	-97.55	337	https://doi.org/10.17190/AMF/1436328
US-ADR	36.77	-116.69	842	https://doi.org/10.17190/AMF/1418680
US-ALQ	46.03	-89.61	-	https://doi.org/10.17190/AMF/1480323
US-Bi1	38.1	-121.5	-2.7	https://doi.org/10.17190/AMF/1480317
US-CZ2	37.03	-119.26	1160	https://doi.org/10.17190/AMF/1419510
US-CZ3	37.07	-119.2	2015	https://doi.org/10.17190/AMF/1419512
US-CZ4	37.07	-118.99	2710	https://doi.org/10.17190/AMF/1419511
US-DPW	28.05	-81.44	23	https://doi.org/10.17190/AMF/1562387
US-EML	63.88	-149.25	700	https://doi.org/10.17190/AMF/1418678
US-Hn2	46.69	-119.46	117.5	https://doi.org/10.17190/AMF/1562389
US-IB1	41.86	-88.22	226.5	https://doi.org/10.17190/AMF/1246065
US-IB2	41.84	-88.24	226.5	https://doi.org/10.17190/AMF/1246066
US-Ivo	68.49	-155.75	568	https://doi.org/10.17190/AMF/1246067
US-Me2	44.45	-121.56	1253	https://doi.org/10.17190/AMF/1246076
US-Me6	44.32	-121.61	998	https://doi.org/10.17190/AMF/1246128
US-Mpj	34.44	-106.24	2138	https://doi.org/10.17190/AMF/1246123
US-Myb	35.05	-121.77	-4	https://doi.org/10.17190/AMF/1246139
US-NGB	71.28	-156.61	5.27	https://doi.org/10.17190/AMF/1436326
US-ORv	40.02	-83.02	221	https://doi.org/10.17190/AMF/1246135
US-OWC	41.38	-82.51	174	https://doi.org/10.17190/AMF/1418679
US-PHM	42.74	-70.83	1.4	https://doi.org/10.17190/AMF/1543377
US-RC1	46.78	-117.08	807	https://doi.org/10.17190/AMF/1498748
US-RC2	46.78	-117.08	799	https://doi.org/10.17190/AMF/1498747
US-RC3	46.99	-118.6	-	https://doi.org/10.17190/AMF/1498749
US-RC4	46.76	-116.95	817	https://doi.org/10.17190/AMF/1498750
US-Rls	43.14	-116.74	1608	https://doi.org/10.17190/AMF/1418682
US-Rms	43.06	-116.75	2111	https://doi.org/10.17190/AMF/1375202
US-Ro1	44.71	-93.09	260	https://doi.org/10.17190/AMF/1246092
US-Ro2	44.73	-93.09	292	https://doi.org/10.17190/AMF/1418683
US-Ro4	44.68	-93.07	274	https://doi.org/10.17190/AMF/1419507
US-Rws	43.17	-116.71	1425	https://doi.org/10.17190/AMF/1375201
US-SCg	33.74	-117.69	465	https://doi.org/10.17190/AMF/1419502
US-SCs	33.73	-117.7	470	https://doi.org/10.17190/AMF/1419501
US-SRG	31.79	-110.83	1291	https://doi.org/10.17190/AMF/1246154
US-SRM	31.82	-110.87	1120	https://doi.org/10.17190/AMF/1246104

US-Seg	34.36	-106.7	1622	https://doi.org/10.17190/AMF/1246124
US-Ses	34.33	-106.74	1593	https://doi.org/10.17190/AMF/1246125
US-Sne	38.04	-121.75	-5	https://doi.org/10.17190/AMF/1418684
US-Srr	38.2	-122.03	8	https://doi.org/10.17190/AMF/1418685
US-StJ	39.09	-75.44	6.7	https://doi.org/10.17190/AMF/1480316
US-Tw1	38.11	-121.65	-9	https://doi.org/10.17190/AMF/1246147
US-Tw3	38.12	-121.65	-9	https://doi.org/10.17190/AMF/1246149
US-Tw4	38.1	-121.64	-5	https://doi.org/10.17190/AMF/1246151
US-Twt	38.11	-121.65	-7	https://doi.org/10.17190/AMF/1246140
US-UMB	45.56	-84.71	234	https://doi.org/10.17190/AMF/1246107
US-UMd	45.56	-84.7	239	https://doi.org/10.17190/AMF/1246134
US-Var	38.41	-120.95	129	https://doi.org/10.17190/AMF/1245984
US-Vcm	35.89	-106.53	3003	https://doi.org/10.17190/AMF/1246121
US-Vcp	35.86	-106.6	2542	https://doi.org/10.17190/AMF/1246122
US-Vcs	35.92	-106.61	2752	https://doi.org/10.17190/AMF/1418681
US-Whs	31.74	-110.05	1370	https://doi.org/10.17190/AMF/1246113
US-Wjs	34.43	-105.86	1931	https://doi.org/10.17190/AMF/1246120
US-Wkg	31.74	-109.94	1531	https://doi.org/10.17190/AMF/1246112
US-Los	46.08	-89.98	480	https://doi.org/10.17190/AMF/1246071
US-MOz	38.74	-92.2	219.4	https://doi.org/10.17190/AMF/1246081
US-Syv	46.24	-89.35	540	https://doi.org/10.17190/AMF/1246106
US-WCr	45.81	-90.08	520	https://doi.org/10.17190/AMF/1246111
US-ARM	36.61	-97.49	314	https://doi.org/10.17190/AMF/1246027
US-Bar	44.06	-71.29	272	https://doi.org/10.17190/AMF/1246030
US-GLE	41.37	-106.24	3197	https://doi.org/10.17190/AMF/1246056
US-Ho1	45.2	-68.74	60	https://doi.org/10.17190/AMF/1246061
US-KFS	39.06	-95.19	310	https://doi.org/10.17190/AMF/1246132
US-KLS	38.77	-97.57	373	https://doi.org/10.17190/AMF/1498745
US-Men	43.08	-89.4	260	https://doi.org/10.17190/AMF/1433375
US-NC2	35.8	-76.67	5	https://doi.org/10.17190/AMF/1246083
US-NC3	35.8	-76.66	5	https://doi.org/10.17190/AMF/1419506
US-NC4	35.79	-75.9	1	https://doi.org/10.17190/AMF/1480314
US-NR1	40.03	-105.55	3050	https://doi.org/10.17190/AMF/1246088
US-Pnp	43.09	-89.42	260	https://doi.org/10.17190/AMF/1433376
US-Prr	65.12	-147.49	210	https://doi.org/10.17190/AMF/1246153
US-Ton	38.43	-120.97	177	https://doi.org/10.17190/AMF/1245971
US-Ha1	42.54	-72.17	340	https://doi.org/10.17190/AMF/1246059
US-PFa	45.95	-90.27	470	https://doi.org/10.17190/AMF/1246090
US-MMS	39.32	-86.41	275	https://doi.org/10.17190/AMF/1246080

Table S3. Information of [CO_2] towers

Code	Full name	Measurement lab	Reference
AMT	Argyle, Maine	NOAA Global Monitoring Division (GMD)	Andrews et al. (2014)
BAO	Boulder Atmospheric Observatory, Colorado	NOAA GMD	Andrews et al. (2014)
CPS	Chapais, Quebec	Environment and Climate Change Canada, Climate Research Division (Environment Canada)	Worthy et al. (2003)
ESP	Estevan Point, British Columbia	Environment Canada	Worthy et al. (2003)
ETL	East Trout Lake, Saskatchewan	Environment Canada	Worthy et al. (2003)
GCI01	Monroe, Louisiana	The Pennsylvania State University, Department of Meteorology (PennState)	Miles et al. (2018a), Richardson et al. (2017)
GCI02	Grenada, Mississippi		
GCI03	Magee, Mississippi		
GCI04	Millersville, Alabama		
GCI05	Panama City, Florida		
HFM	Harvard Forest, Massachusetts	Harvard University, Division of Engineering and Applied Science, Department of Earth and Planetary Science	Sargent et al. (2018)
HNP	Hanlan's Point, Ontario	Environment Canada	Worthy et al. (2003)
LEF	Park Falls, Wisconsin	NOAA GMD	Andrews et al. (2014)
MBO	Mt. Bachelor Observatory	NOAA GMD & University of Washington	McClure et al. (2016)
MRC	Marcellus Pennsylvania	PennState	Miles et al. (2018a), Miles et al. (2018b)
OSI	Silverton, Oregon	Oregon State University, Department of Forest Science	Schmidt et al. (2016)
SCT	Beech Island, South Carolina	NOAA GMD & Savannah River National Laboratory	Andrews et al. (2014)
SGP	Southern Great Plains, Oklahoma	Lawrence Berkeley National Laboratory and ARM Climate Research Facility	Biraud et al. (2013), Torn et al. (2011)

SNP	Shenandoah National Park	NOAA GMD & University of Virginia	Andrews et al. (2014), Lee et al. (2012), Lee et al. (2012)
TPD	Turkey Point, Ontario	Environment Canada	
WBI	West Branch, Iowa	NOAA GMD	Andrews et al. (2014)
WGC	Walnut Grove, California	NOAA GMD & Lawrence Berkeley National Laboratory, California Greenhouse Gas Emission Measurement Project, Environmental Energy Technologies Division	Andrews et al. (2014)
WKT	Moody, Texas	NOAA GMD	Andrews et al. (2014)

References:

Andrews, A. E., Kofler, J. D., Trudeau, M. E., Williams, J. C., Neff, D. H., Masarie, K. A., et al. (2014). CO2, CO, and CH4 measurements from tall towers in the NOAA Earth System Research Laboratory's Global Greenhouse Gas Reference Network: instrumentation, uncertainty analysis, and recommendations for future high-accuracy greenhouse gas monitoring efforts. *Atmospheric Measurement Techniques*, *7*(2), 647–687. https://doi.org/10.5194/amt-7-647-2014

McClure, C. D., Jaffe, D. A., & Gao, H. (2016). Carbon Dioxide in the Free Troposphere and Boundary Layer at the Mt. Bachelor Observatory. *Aerosol and Air Quality Research*, *16*(3), 717–728. https://doi.org/10.4209/aaqr.2015.05.0323

Miles, N. L., Richardson, S. J., Martins, D. K., Davis, K. J., Lauvaux, T., Haupt, B. J., & Miller, S. K. (2018). ACT-America: L2 In Situ CO2, CO, and CH4Concentrations from Towers, Eastern USA. https://doi.org/doi.org/10.3334/ORNLDAAC/1568.

Miles, Natasha L., Martins, D. K., Richardson, S. J., Rella, C. W., Arata, C., Lauvaux, T., et al. (2018). Calibration and field testing of cavity ring-down laser spectrometers measuring CH_4, CO_2, and $\delta^{13}CH_4$ deployed on towers in the Marcellus Shale region. *Atmospheric Measurement Techniques*, *11*(3), 1273–1295. https://doi.org/10.5194/amt-11-1273-2018

Sargent, M., Barrera, Y., Nehrkorn, T., Hutyra, L. R., Gately, C. K., Jones, T., et al. (2018). Anthropogenic and biogenic CO2 fluxes in the Boston urban region. *Proceedings of the National Academy of Sciences*, *115*(29), 7491–7496. https://doi.org/10.1073/pnas.1803715115

Schmidt, A., Law, B. E., Göckede, M., Hanson, C., Yang, Z., & Conley, S. (2016). Bayesian Optimization of the Community Land Model Simulated Biosphere-Atmosphere Exchange using CO2 Observations from a Dense Tower Network and Aircraft Campaigns over Oregon. *Earth Interactions*, *20*, 1–35. https://doi.org/10.1175/EI-D-16-0011.1

Worthy, D. E. J., Higuchi, K., & Chan, D. (2003). North American influence on atmospheric carbon dioxide data collected at Sable Island, Canada. *Tellus B: Chemical and Physical Meteorology*, *55*(2), 105–114. https://doi.org/10.3402/tellusb.v55i2.16731